Available online at www.sciencedirect.com
SCIENCE DIRECT®
Composites Science and Technology 65 (2005) 1052–1068
COMPOSITES SCIENCE AND TECHNOLOGY
www.elsevier.com/locate/compscitech

Dynamic fracture behavior of model sandwich structures with functionally graded core: a feasibility study

M.S Kirugulige, R. Kitey, H.V. Tippur *

Department of Mechanical Engineering, Auburn University, 202 Ross Hall, AL 36849, USA

Received 25 April 2004; received in revised form 28 September 2004; accepted 14 October 2004
Available online 12 January 2005

Abstract

Feasibility of introducing compositional gradients to the core of a sandwich structure and the resulting fracture behavior under impact loading conditions is the primary focus of the study. Model sandwich structures comprising of graded core with bilinear variation of volume fraction of hollow microballoons are considered for experimental and numerical simulations. Conventional sandwiches with homogeneous core are also developed for comparison. The crack tip in both configurations is positioned such that global as well as local material characteristics are matched in both models. Dynamic mode-I crack tip deformations are mapped experimentally using optical interferometry and high-speed photography. Measurement of fracture parameter histories is used to demonstrate equivalence between graded and conventional architectures. The fracture behavior in sandwich core is explained using independent experimental results obtained from monotonically graded foam sheets. The measurements up to crack initiation are also used to validate finite element models. The numerical models are subsequently used in a parametric study of different elastic impedance gradients in the core on mixed-mode fracture performance of graded sandwich structures having a crack at the face-sheet/core interface under stress-wave loading conditions. The results show significant reduction in stress intensification in the presence of compositional gradients when compared to conventional constructions.

Keyword: Sandwich structures

1. Introduction

Sandwich constructions are extensively used in engineering for achieving strong, stiff and light-weight structures. Availability of a wide selection of face-sheet and core materials make it possible to derive multi-functional benefits pertaining to acoustic, thermal, dielectric, and energy dissipation characteristics [1] as well. Among the many applications where sandwich constructions have been successfully used include ship hulls, aircraft structures, high-speed trains, engineered materials for building materials and cargo containers. In the near future, sandwich architecture is anticipated to enter the next generation cargo transports, naval structures and spacecrafts provided further improvements are made.

Past studies [2–5] suggest that failure response of sandwich structures under impact loading conditions need further improvement. Conclusions drawn based on post-mortem analyses and/or follow-up mechanical testing of damaged sandwich structures point out that extensive face-sheet/core delamination, face-sheet damage, shear cracking occur in sandwich structures when subjected to impact. Understanding the sequence of failure events after impact is critical for improving response of sandwich structures but has remained elusive due to the difficulty of monitoring internal damage and failure evolution in real-time during stress-wave loading. This has been recently overcome by Xu and Rosakis [6] using

* Corresponding author.
E-mail address: htippur@eng.auburn.edu (H.V. Tippur).

0266-3538/$ - see front matter © 2004 Elsevier Ltd. All rights reserved.
doi:10.1016/j.compscitech.2004.10.029

sandwich configurations made of transparent model materials and using photoelasticity and high-speed photography. They have been able to successfully describe the chronology of various complex failure events during impact loading. Their work points to the occurrence of interfacial fracture between the face-sheets followed by crack kinking into and branching in the core, prior to total failure.

Thus, any further enhancement of sandwich structural performance for critical applications should potentially include new ideas capable of minimizing some of the aforementioned failure modes without compromising existing benefits. This can be potentially accomplished by incorporating novel material construction concepts as well as newer class of materials for the face sheets and the core. Based on these motivating factors, the current work examines the feasibility of (a) utilizing functional/compositional grading of the core in a sandwich structure, and (b) using high-performance core materials such as syntactic foams for sandwich construction.

In regards to functional grading, advanced material processing methods developed in recent years have made it possible to introduce compositional gradients in many material systems [7–10]. The resulting materials with spatial variations in properties are collectively referred to as Functionally Graded Materials or FGM. A typical FGM includes nano- and/or micro-scale filler/s suitably dispersed in a matrix material. In them, volume fraction, morphology and/or bonding characteristics of the constituents are spatially varied to achieve the required functionalities. Advantages of introducing compositional gradients into the core of sandwich structures include failure mitigation and improved load bearing capacity by eliminating sudden jumps in the material properties. A recent theoretical analysis of statically loaded sandwich beams with a functionally graded core [11] indeed demonstrates that graded cores significantly reduce face-sheet/core interfacial shear stresses. In a different study, using finite element analysis, Nakamura and Wang [12] have demonstrated that suppression of impact damage in graded materials is also possible. Their work clearly demonstrates the possibility of reducing and redirecting microcracks if functionally graded layers are used. Earlier studies by Tippur and his coworkers [13–15] have noted several fracture related benefits of compositional grading under low-velocity loading conditions. Monotonically graded glass-filled epoxy particulate composites studied using optical interferometry and strain gages have shown that it is possible to lower crack tip loading rates, delay crack initiation and enhance overall fracture toughness in graded structures. Using a discretely layered model structure with a stepwise increase in nonlinearity, Parameswaran and Shukla [16] have shown that crack jump across the layers diminish during dynamic propagation.

Improvements in sandwich structural performance can also be potentially achieved by using different material systems for the core instead of conventional polymeric foams. One such material system includes syntactic foams. Syntactic foams, initially developed for deep-sea applications, have drawn the attention of other disciplines in recent times [17,18]. The superiority of syntactic foams is due to the fact that porosity in these materials is typically microscopic (typically tens of micrometers) in nature and the resulting surface area to volume ratio of the pores is known to enhance mechanical performance, particularly the compressive and shear responses [19]. Superior dielectric, thermal, fire resistant and hygroscopic characteristics add to the list of advantages as well. The possibility of cost-effective fabrication of core materials over a wide range of mass densities by simply dispersing pre-fabricated hollow microballoons in a suitable matrix material is quite attractive. The availability of a wide range of microballoons of different sizes and materials (carbon, ceramic, phenolic) also adds to the resulting multifunctional benefits. The hollow microballoons with sub-micron wall thickness could prove advantageous from the view point of nano-scale mechanics. Further, material anisotropy typical of conventional core materials such as polymeric foams, honeycombs [20], and naturally occurring porous materials such as balsa wood [21] are absent in syntactic foams which are macroscopically isotropic, thereby simplifying mechanical design. When microballoons of extremely small wall thickness relative to diameter are used in matrix, they can also be approximated as simple porous materials [22]. In recent years, advantages of using syntactic foam as the core material for impact related applications are recognized by a few investigators [23–25]. The ability of these foams to contain the damage to a small area and high specific energy absorption characteristics are noted.

Thus, the current work is aimed towards examining the feasibility of extending the concept of functional grading using syntactic foams as a core material for sandwich structures and examining the resulting advantages, if any. In the next section, preparation and elastic characterization of syntactic foam core materials are described. The experimental methodology used for preparing homogeneous foam as well as the ones with monotonic and bilinear compositional grading is detailed. The mode-I fracture experiments involving optical interferometry and high-speed photography for real-time recording of failure evolution are outlined in Section 3. This is followed by a description of experimental results in all categories of specimens in Section 4. In Section 5, finite element (FE) simulations, used to supplement experimental situations, are described. After comparing experiments with numerical simulations successfully, FE simulations are extended to provide limited explanation of experimental observations and subsequently sim-

ulate mixed-mode crack configurations that are relatively challenging to study experimentally. Results for two such configurations with mixed-mode cracks at the face-sheet/core interface are presented in Section 6 to bring out possible advantages of functional grading. The observations and results are discussed and summarized in Sections 7 and 8, respectively.

2. Materials processing and characterization

2.1. Homogeneous foam

In this study, syntactic epoxy foams of various volume fractions were used as the core material. A brief description of preparation and elastic characterization of these foams is presented in the following. Homogeneous syntactic epoxy foam sheets with randomly distributed microballoons were first prepared. The microballoons used in this investigation were commercially available *hollow* glass spheres (Surface treated Type K-1 hollow microballoon from 3M, Inc., USA) of mean diameter ~60 μm and wall thickness ~600 nm. Low-viscosity epoxy resin (Reformulated (2003) Epo-Thin™ from Beuhler, Inc., resin to hardner ratio of 100:36 by weight) having low shrinkage and long duration room temperature curing characteristics was used as the matrix material. The material preparation consisted of mixing a predetermined amount of microballoon volume fraction into the epoxy material. The microballoons were carefully stirred into the epoxy resin while avoiding air bubbles and agglomeration. Stirring of the mixture was continued until the mixture showed a tendency to gel and then poured into molds. This helped to eliminate any buoyancy induced floating of the microballoons during subsequent curing. The mixture was cured for 72 h under laboratory conditions. The cured material with randomly but uniformly distributed microballoons – sheets of nominal dimensions 152 mm × 100 mm × 8 mm – was further rested for a week prior to testing. The elastic and physical characteristics as a function of volume fraction of the dispersant were determined. The volume fraction, V_f, of the microballoons in these sheets ranged between 0% and 45%. The longitudinal (C_L) and shear (C_S) wave speeds of these sheets were determined using ultrasonic pulse-echo method (see [9] for details) using 10 and 5 MHz transducers (Panametric, Inc.), respectively. The mass density ρ of each composition was also determined by measuring the weight and the volume of cured material. The values of elastic moduli (E) and Poisson's ratio (ν) were then determined using measured wave speeds and mass density [9]. The resulting elastic modulus and mass density variations with volume fraction of microballoons are shown in Fig. 1(a). Both quantities reduce monotonically with microballoon volume fraction over the entire range. The values of Poisson's ratio in these compositions were found to be nearly constant at 0.35 ± 0.02.

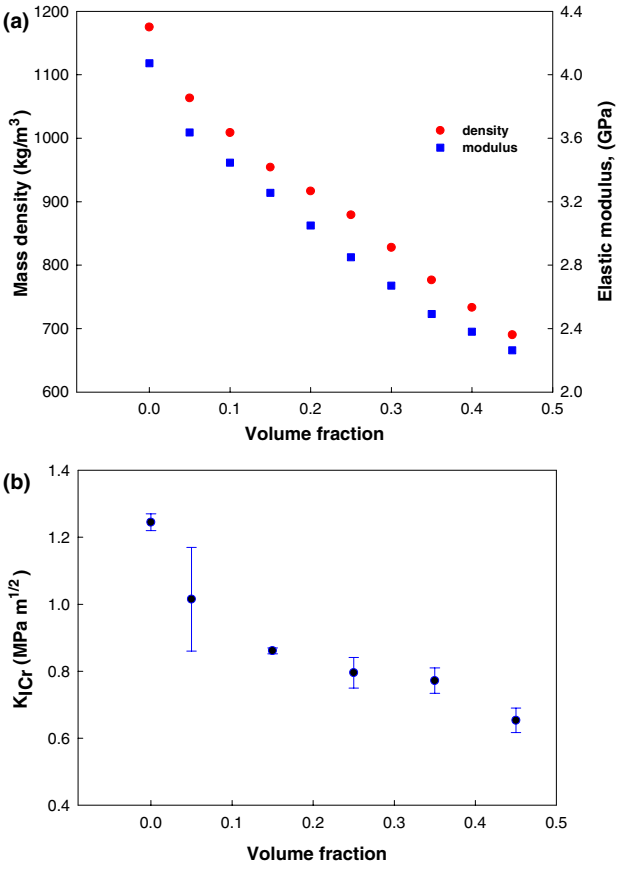

Fig. 1. Material properties of epoxy syntactic foams: (a) variation of mass density and dynamic elastic modulus with microballoon volume fraction; (b) variation dynamic initiation toughness (impact velocity = 2 m/s) with microballoon volume fraction for epoxy syntactic foams.

Mode-I crack initiation toughness tests were also conducted on homogeneous compositions. Beam samples (152 mm × 27 mm and 7.5 mm thickness) from homogeneous syntactic foam sheets with different microballoon volume fractions (0%, 5%, 15%, 25%, 35% and 45%) were prepared. Edge crack of length 5.4 mm ($a/W = 0.2$) was cut along the mid-span in each of these samples. Dally–Sanford single strain gage method [26] was used to obtain dynamic stress intensity factor for homogeneous syntactic foam samples. [1] A strain gage of gage length 0.8 mm (CEA-13-032WT-120 from Vishay-Micromeasurements Group, Inc.) was located radially at a distance of 4 mm from the crack tip and at an angle of 60° to the crack orientation. These specimens were impact loaded (impact velocity = 2 m/s)

[1] This approach provides a better estimation of crack initiation toughness when compared to the method used in [14] wherein measured peak-load values recorded during impact were utilized. This is because the assumption that peak-load occurs at crack initiation need not have to be made.

in 3-point bend configuration. Strain history recorded by the strain gage is used to obtain the crack initiation toughness values. Details are avoided here for brevity and can be found elsewhere in [27]. Fig. 1(b) shows the variation of mode-I dynamic initiation toughness (K_{Icr}) with microballoon volume fraction. Monotonic reduction in the crack initiation toughness values with volume fraction can be seen from this figure. Approximately 50% reduction in fracture toughness can be noted when microballoon volume fraction increases from 0% to 45%. A similar percentage reduction in Young's modulus and mass density over the same range of volume fraction is also evident.

2.2. Graded foam with monotonic volume fraction variation

Before studying the fracture behavior of sandwich structures with functionally graded core, feasibility of processing graded foam material comprising of specific microballoons and its fracture behavior had to be understood. Accordingly, graded syntactic foam sheets with volume fraction varying from 0% to 45% of microballoons in the epoxy binder were prepared. The methodology used for processing graded foams consisted of preparing several different homogeneous epoxy-microballoon mixtures. Nine different mixtures with 5–45% in uniform steps of 5% were prepared separately. The mixtures were transferred into the mold sequentially, at a state somewhat less viscous than the ones for the homogeneous foams, described in Section 2.1. The mixture with the lowest volume fraction of microballoons was poured first into the mold followed by the next higher volume fraction, and so on. Each layer was nominally 5 mm thick. A complex interplay of buoyancy and viscous forces on the microballoons along with thermal convection during polymerization results in a nearly linear volume fraction gradient. The gradient extends over approximately 45 mm, between a region of nearly pure epoxy at one end and microballoon-rich epoxy on the other in specimens with dimensions 152 mm × 45 mm × 8 mm. The variations in mechanical properties in these specimens over the sample width were estimated by using look-up charts presented in Fig. 1(a). These charts in conjunction with local longitudinal and shear wave speeds at various locations along the width of the graded foam castings were used to determine mass density and elastic modulus variations. These are shown in Fig. 2 and they generally follow an approximately linear trend.

2.3. Foam core with bilinear volume fraction variation for sandwich structures

The material processing of bilinearly graded core for sandwich structures required preparation of two monotonically graded syntactic foam sheets with identical linear variations in microballoon volume fraction over half-width of the core. The material property variations were introduced using techniques developed for monotonically graded core material described above. The primary difference in this category was the thickness of each layer of the mixture poured into the mold during sample preparation. It was 2 mm and the layers included nine compositions with 5–45% in uniform steps. Upon curing, the graded sheet was machined to 152 mm × 18 mm × 8 mm dimension with 45% volume fraction layer of 2 mm. Two such monotonically graded halves of the core were subsequently bonded along the compliant edges using a mixture of the corresponding volume fraction (45% in this case) to form the completed core having outer epoxy-rich and inner microballoon-rich regions. The core was subsequently sandwiched between epoxy face-sheets (each 3 mm) by directly casting epoxy onto the core on both sides and machining the sample to its final dimensions of 152 mm × 42 mm × 8 mm. A conventional sandwich structure of exactly same dimensions but with a homogeneous core was also prepared for comparative testing. Both conventional and graded sandwich structures with their bilinear variation in properties are schematically shown in Fig. 3. The actual variation of elastic modulus is shown on the left vertical

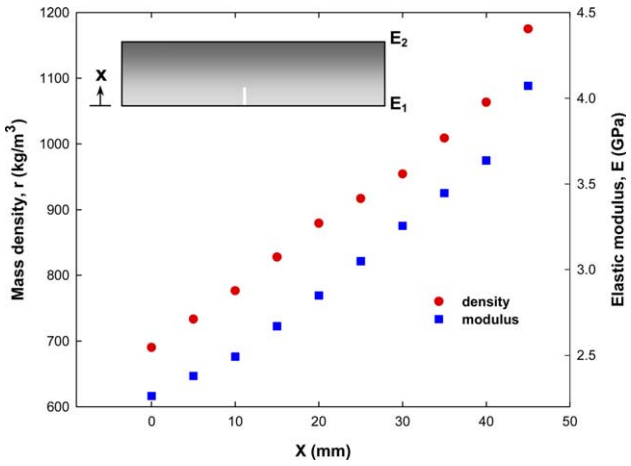

Fig. 2. Property variations in graded foam with monotonic volume fraction variation.

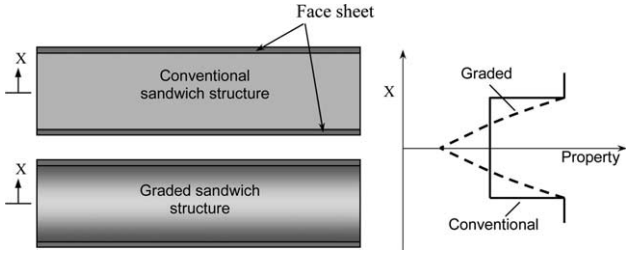

Fig. 3. Schematic depicting property variations in conventional and graded foam core sandwich structures.

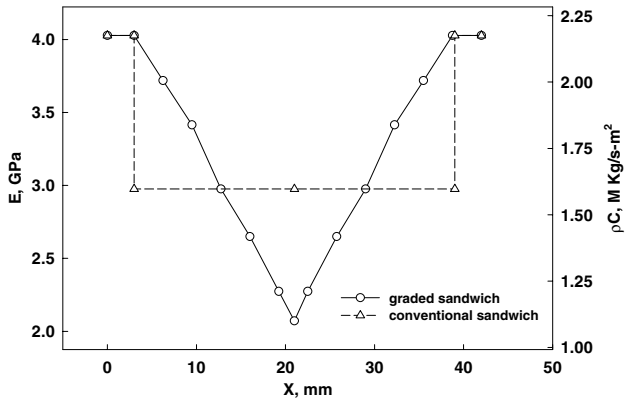

Fig. 4. Variation of Elastic modulus and elastic impedance along the specimen width (face sheet + core) for both conventional and graded sandwich structures.

axis of Fig. 4 for graded as well as conventional sandwich structures. Also shown in this figure is the variation of the property ρC or $\sqrt{E\rho}$ with sample width along the right vertical axis.

2.4. Equivalency of homogeneous and graded sandwich core

Any two structures being compared can be equivalent in terms of weight, stiffness, strength or a combination of two or more of such features. In the reported literature, investigations into the mechanical performance of functionally graded materials generally involve studying stress distribution and related engineering parameters when properties vary in the medium according to simple laws (power law and exponential type variations are common). Most studies to date have focused on evaluating stresses when elastic gradients exist in the medium. For example, Bao and Cai [28], Lee and Erdogan [29], Gu and Asaro [30] and Marur and Tippur [31] have all examined the role of elastic modulus gradients on crack tip stress intensity factors in their numerical studies under quasi-static loading conditions. Under dynamic loading conditions, influence of elastic gradient profiles described in terms of spatial variation of elastic wave speeds have been studied by Rousseau and Tippur [14] for mode-I loading. In this work, mechanical performance of a cracked conventional and a cracked functionally graded sandwich structure subjected to impact loading were comparatively studied in terms of stresses and stress intensity factor histories. Hence, unlike in the previous works, elastic impedance, $\sqrt{E\rho}$, was used for developing equivalent sandwich architectures. The choice was guided by the fact that elastic impedance ($=\rho C$) of the material scales directly with the stresses under elasto-dynamic loading conditions [32].

The conventional structure consisted of central foam core sandwiched between two face-sheets. For simplicity of experimental and numerical simulations, face-sheets were made of epoxy sandwiching a central core made of epoxy based syntactic foam of a known volume fraction resulting in a structure having relatively stiff face sheets with compliant core. The graded sandwich structure, on the other hand, had a functionally graded core with epoxy-rich layer adjacent to the face-sheets and gradually becoming microballoon-rich foam in the interior of the structure (see, Fig. 3). The two structures were designed such that the average values of the 'property' over the core thickness of the graded and conventional architectures were same, specifically the elastic impedance $\overline{\rho C} = \frac{1}{W}\int_0^W C(X)\rho(X)\,\mathrm{d}X$, where W is the specimen height and X denotes the spatial variable as shown and the over-bar denotes average value. The variation of ρC along the width of the specimen is shown in Fig. 4. For the resulting variations the value of $\overline{\rho C}$ for the graded sandwich structure is 1.65 M kg/s m^2. Using this value, the corresponding constant volume fraction to be used in case of a conventional sandwich construction was determined and was found to be same as the foam with approximately 25% of microballoons.

3. Experiments: mode-I loading

In the mid-region of each of the samples, a thin layer of aluminum was transferred onto a 152 mm × 42 mm or 152 mm × 45 mm face for performing optical interferometry. Edge crack of length $a/W = 0.16$ was machined (root radius ~150 μm) into monotonically graded specimens and $a/W = 0.31$ in case of sandwich structures using a diamond impregnated circular saw. The crack length in the latter was such that the crack tip location in both graded and conventional samples were at a location where the local properties were identical ($V_f = 0.25$). This, along with equal average values of elastic impedance over the sample width, ensured equality of local and global properties in the two samples. Thus, differences in dynamic fracture behavior, if any, would be attributable directly to the compositional gradations. Dynamic fracture tests on these samples were carried out under low-velocity (5.8 m/s) impact loading conditions. All samples were subjected to single-point symmetric impact at the mid-span on the 152 mm × 8 mm face in free–free beam configuration.

The optical methods of Coherent Gradient Sensing (CGS) in conjunction with high-speed photography [33,14] were used in this study to perform real-time measurement of instantaneous surface deformations around the crack tip. A schematic of the optical set-up is shown in Fig. 5. The measurement system consisted of an impactor, pulse-laser, CGS interferometer and a continuous access high-speed camera. During the experiment, a pneumatically operated impactor-head was launched towards the specimen. During its descent, it first triggered a photo-detector to open a capping shutter located

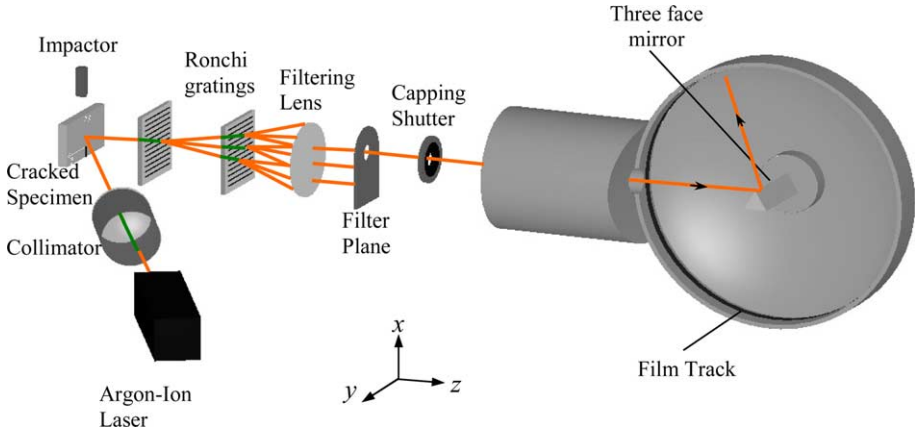

Fig. 5. Schematic of reflection CGS and high-speed photography set-up.

in front of the high-speed camera, allowing light to reach its internal cavity. When the impactor-head contacted the specimen, it closed an electrical circuit initiating a series of laser pulses for a duration corresponding to a single sweep of the laser beam on a stationary film track. The light entering the camera was reflected-off of a spinning three-facet mirror mounted on a turbine shaft. The reflected light beam was swept on the film held in a track as discrete images. At the end of that period, the capping shutter was closed to prevent over-writing on the film. In the current experiments, the laser pulse was repeated every 5 μs with a pulse width of 50 ns and a total recording duration of approximately 320 μs.

A collimated argon-ion laser beam (~50 mm diameter) was used to illuminate the specimen made specularly reflective in the region of interest. The reflected light off the specimen surface carries information about the local surface deformations. The light beam was processed using a lateral shearing interferometer, CGS, comprising of a pair of Ronchi gratings (25 μm pitch, chrome on glass gratings) and a Fourier filtering/imaging lens. The resulting fringes represent surface slopes in the x-direction. Using governing equations of reflection CGS, and plane stress approximation, optical measurements can be related to interference fringes using,

$$\frac{\partial w}{\partial x} \approx \frac{\delta w}{\delta x} = \frac{\delta\left[-\frac{\nu B}{2E}\left(\sigma_x + \sigma_y\right)\right]}{\delta x} = \frac{Np}{2\Delta}, \quad N = 0, \pm 1, \pm 2, \ldots, \tag{1}$$

where N denotes fringe orders, p is the pitch of the gratings (25 μm), Δ is the grating separation distance (49 mm), B is the specimen thickness and $\delta(\cdot)$ is the difference operator.

3.1. Monotonically graded foam sheets

Experiments on monotonically graded foam sheets included two types: (a) crack on the stiffer side of the core material with impact occurring on the compliant side and (b) crack on the compliant side of the core material with impact occurring on the stiffer side. Denoting the elastic modulus of the edge of the cracked sheet behind the crack tip as E_1 and the one ahead of the crack as E_2 the former corresponds to $E_2 < E_1$ and the latter to $E_2 > E_1$ The resulting interference fringes for the two cases are shown in Figs. 6(a) and (b). For each case representative interferograms corresponding to pre- and post-initiation instants are included. The legends correspond to the time instant at which the image was recorded after impact. At earlier times severe concentration of interference fringes are seen at the impact location (near the top edge) while only a few fringes are seen at the crack tip (near the bottom edge). With the passage of time crack tip deformation increases, as evidenced by the increasing number of fringes at the crack tip, followed by crack initiation and growth. Fringe pattern in each case is symmetric on either side of the crack, indicating mode-I deformations. (Each image shows a vertical line drawn parallel to the initial crack at a distance of 10 mm for subsequent analysis of fringes that requires magnification factor.)

3.2. Sandwich structures with graded and homogeneous foam core

Optically measured deformations in cracked sandwich structures with homogeneous and graded core material are shown in Figs. 7(a) and (b), respectively. Again, instant at which the image was captured after impact is shown underneath each image. The impact occurs at the top edge of the specimen and the pre-crack is situated at the lower end of the image. The evidence of two-halves of individually cast homogeneous and graded core strips bonded along a horizontal plane at the middle of the specimen can also be seen in Figs. 7(a) and (b). The crack length in each case is chosen such that the crack tip is located in the core material where the volume fraction of the microballoons is identical in both configurations. Interferograms corresponding to

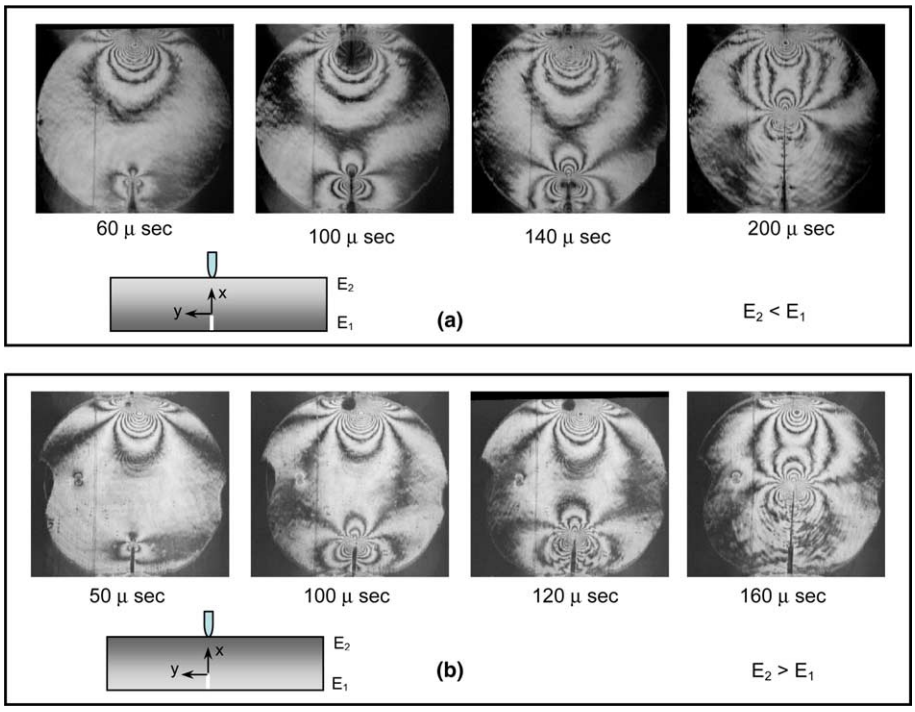

Fig. 6. Selected CGS interferograms representing contours of $\frac{\delta w}{\delta x}$ in functionally graded epoxy syntactic foam sheet impact loaded on the edge opposing the crack tip. (The vertical line is at a distance of 10 mm from the crack.) (a) Crack on stiffer side $E_2 < E_1$ and (b) crack on compliant side $E_2 > E_1$. Fringe sensitivity ~0.015°/fringe.

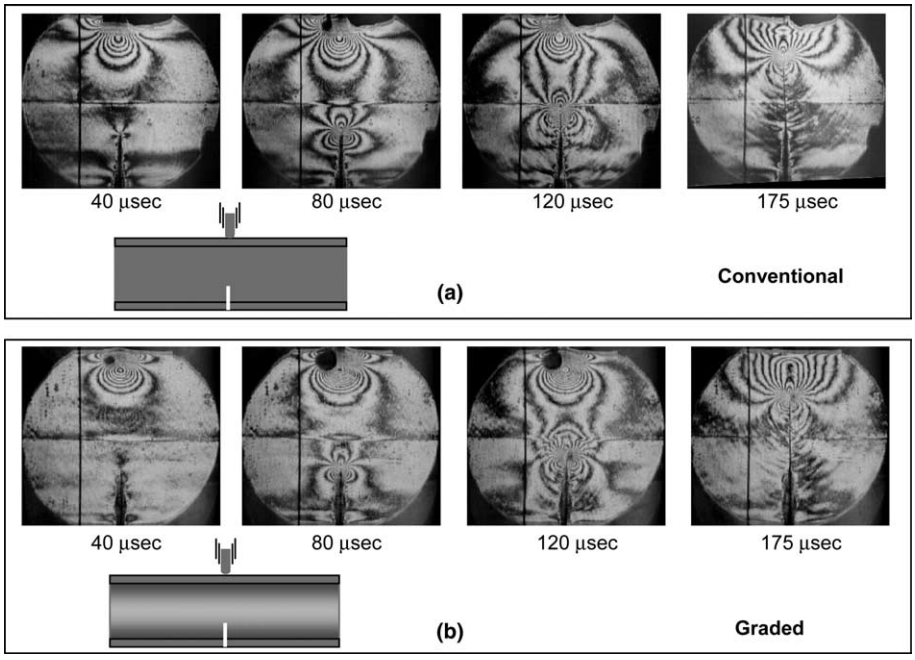

Fig. 7. Representative CGS interferograms representing contours of $\frac{\delta w}{\delta x}$ in (a) conventional, (b) graded sandwich structures, impact loaded on edge opposite to the crack tip. (The vertical line is at a distance of 10 mm from the crack). Fringe sensitivity ~0.015°/fringe.

both pre- and post-crack initiation events are included. Immediately after impact, the interference fringes representing surface slopes in the direction of the crack orientation are visible only near the impact point while the crack tip region is relatively free from interference fringes. With passage of time, the crack tip experiences stress waves and progressively deforms leading to crack initiation and dynamic crack growth. The crack tip fringes in each case are generally symmetric about the crack plane suggesting dominant mode-I deformations.

(It should be noted that the dark spot at the impact location in each case is due to the limited aperture size and alignment of optics and does not influence the crack tip fringes.)

Fig. 8 shows photographs of fractured specimens in the mid-portion of the sheet on either sides of the crack path. The crack growth in these photographs occurs from the bottom to the top predominantly in a mode-I fashion in the core region. Interestingly, clear evidence of interfacial separation between the face-sheet and the core material can be seen when conventional architecture is tested while no evidence of the same is seen when graded core is used.

3.3. Fringe analysis

The interferograms were used for identifying instantaneous crack tip location during the event window. Using this information, crack speed history was determined by differentiating crack length history with respect to time using a central difference scheme. The crack tip stress intensity factors were also extracted from the interference patterns (Eq. (1)) using over-deterministic least-squares analysis of optically measured surface slope data in conjunction with crack tip field descriptions available for graded materials. The details of fringe digitization and analysis are avoided here for brevity and can be found elsewhere [33]. Pre-crack initiation interferograms were analyzed using asymptotic crack tip expressions for stresses in a planar nonhomogeneous elastic body. Using asymptotic analysis, the first two terms of such a description for the sum of in-plane normal stresses near a quasi-statically loaded mode-I stationary crack in a nonhomogeneous sheet has been shown to be of the form [34],

$$(\sigma_x+\sigma_y)=(C_0 r^{-\frac{1}{2}} f_0^{\mathrm{I}}(\theta)+C_1 r^0 f_1^{\mathrm{I}}(\theta))+\mathrm{O}(r^{\frac{1}{2}}), \tag{2}$$

where (r,θ) denote crack tip polar coordinates, $f_0^{\mathrm{I}}, f_1^{\mathrm{I}}$ are angular functions, and C_0 and C_1 are the coefficients of the expansion with $C_0=\frac{K_{\mathrm{I}}}{\sqrt{2\pi}}$, K_{I} being the mode-I stress intensity factor. It should be noted that the angular functions for the first two terms in Eq. (2) are identical to the ones for a homogeneous counterpart. Using plane stress assumptions, out-of-plane displacement w can be related to in-plane stresses using Eq. (1). Eq. (2) in conjunction with Eq. (1) was used for determining stress intensity factors from the interferograms with an implicit assumption that all inertial effects enter the analysis through coefficients of the asymptotic field.

Post-crack initiation fringe patterns were analyzed using explicit field descriptions for a growing crack based on the observations reported in Rousseau and Tippur [14]. For the sake of completeness, expressions for the instantaneous sum of in-plane normal stresses in nonhomogeneous materials are given [34],

$$\begin{aligned}(\sigma_x+\sigma_y)\approx\frac{-v}{2(1+v)(1-2v)}\Bigg\{&A_0(t)r_l^{-\frac{1}{2}}\cos\frac{\theta_l}{2}+A_1(t)\\&+A_2(t)r_l^{\frac{1}{2}}\cos\frac{\theta_l}{2}-\frac{\alpha}{4\alpha_l^2}A_0(t)r_l^{-\frac{1}{2}}\cos\frac{3\theta_l}{2}\\&+\frac{2\alpha\alpha_s}{(k+2)(\alpha_l^2-\alpha_s^2)}B_0(t)r_s^{\frac{1}{2}}\cos\frac{\theta_s}{2}\Bigg\},\end{aligned} \tag{3}$$

where

$$k=\frac{\lambda_0}{\mu_0},\quad \alpha_l=\sqrt{1-\frac{\rho_0 c^2}{\mu_0(k+2)}},\quad \alpha_s=\sqrt{1-\frac{\rho_0 c^2}{\mu_0}},$$

$$r_l=\sqrt{x^2+\alpha_l^2 y^2},\quad \theta_l=\tan^{-1}\frac{\alpha_l y}{x},$$

$$r_s=\sqrt{x^2+\alpha_s^2 y^2},\quad \theta_s=\tan^{-1}\frac{\alpha_s y}{x},$$

$$A_0=\frac{(1+\alpha_s^2)(1-\alpha_l^2)}{4\alpha_s\alpha_l-(1+\alpha_s^2)^2}\frac{K_{\mathrm{I}}}{\mu\sqrt{2\pi}},\quad B_0=\frac{2\alpha_l}{1+\alpha_s^2}\frac{1-\alpha_s^2}{1-\alpha_l^2}A_0.$$

In the above, c is the crack speed, λ is Lamé's constant and A_0, A_1 and A_2 are unknown coefficients of the

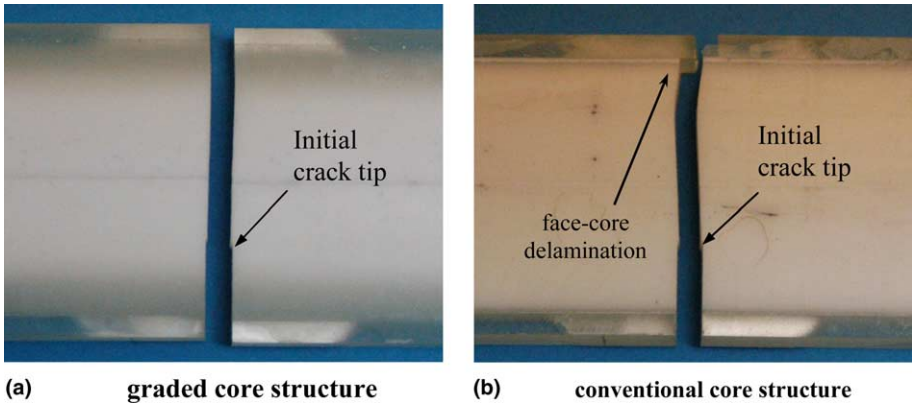

Fig. 8. Photographs showing fractured (a) graded and (b) conventional sandwich structure specimens from optical tests.

asymptotic series. In deriving Eq. (3) material nonhomogeneity is assumed to be of the form, $\mu = \mu_o \exp(\alpha\xi)$ and $\rho = \rho_o \exp(\alpha\xi)$, where μ and ρ denote shear modulus and mass density, the subscript 'o' designates the original crack tip location (origin of the ξ-axis), and nonhomogeneity parameter α is a scalar. For steady state conditions, location of the moving crack tip at any instant in time is defined at the origin of the x–y axes. Evidently, as the material gradient parameter α becomes zero, the equations reduce to that of its homogeneous counterpart. As noted in [14], the last term in the above equation, becomes unbounded in the limit the crack speed approach zero but behaves normally at nominal crack speeds. More importantly, it has been shown in [14] that for relatively shallow elastic gradients such as the ones used in the current study, the results would not be greatly affected when a *locally homogeneous crack tip behavior* is utilized for fringe analysis. That is, by analyzing the data in the close vicinity of the crack tip (yet beyond the crack tip triaxiality zone of $r/B \sim 0.35$, $90° < \theta < 135°$) as outlined in [14], the differences in the values of dynamic mode-I stress intensity factors were about 5%. Accordingly, a locally homogeneous material behavior ($\alpha = 0$ in Eq. (3)) is used for extracting the mode-I stress intensity factors. The quality of the least-squares fit of the data is used for attesting the accuracy of the approach.

4. Experimental results

4.1. Monotonically graded foams

Instantaneous crack length and normalized crack velocity histories for two different cases of monotonically graded foam sheets are shown in Figs. 9(a) and (b). The crack initiation occurs earlier in case of the specimen with a crack on the compliant side ($E_2 > E_1$) when compared to the one with a crack on the stiffer side ($E_2 < E_1$). Upon initiation, crack growth is essentially continuous during the observation window. The normalized crack speed histories show that the crack accelerates following initiation to a maximum value followed by an oscillatory behavior as the crack is driven forward by discrete wave reflections from the boundaries of the specimen. Sudden acceleration after initiation is attributed to the finite root radius (~150 μm) of the initial crack inserted into the samples. The data suggests that the average crack speeds ($\sim 0.35 C_R$ for $E_2 > E_1$ and $\sim 0.29 C_R$ for $E_2 < E_1$ with C_R being the Rayleigh wave speed) are higher when the crack is on the compliant side of the specimens.

The stress intensity factors for the two cases of the graded foam sheets were extracted using over-deterministic least-squares analysis. Each fringe pattern was digitized and fringe orders and fringe location data was

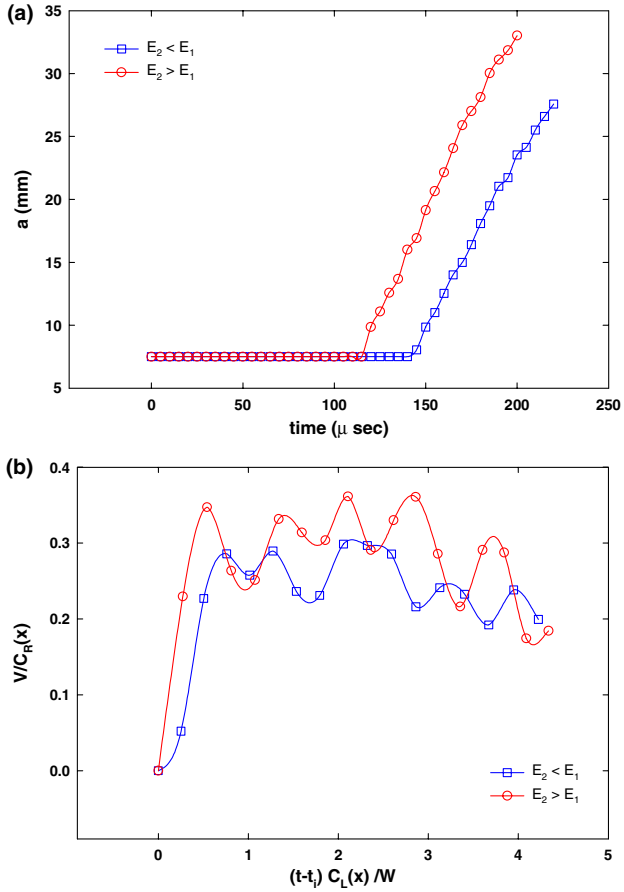

Fig. 9. Crack growth behavior in graded foam specimens under impact loading. (a) Crack growth history, (b) normalized crack speed histories (t = time from impact, t_i = time at crack initiation, and C_L and C_R are longitudinal and Rayleigh wave speeds).

collected. A typical result for monotonically graded foam with crack on compliant side is shown as an inset in Fig. 10. Digitized experimental data (symbols) and the least-squares fit (solid line) shown in the figure are for 100 μs time instant after impact. The least-squares fit considering K-dominant solution shows good agreement with the optical data.

The stress intensity factor histories thus obtained are shown in Fig. 10. In each case, crack tip stress intensification is evident only after ~50 μs after impact due to finite resolution of the optical technique. The stress intensity factors monotonically increase until crack initiation (indicated by vertical bands in the plot). The crack initiates earlier when situated on the compliant side of the sheet ($E_2 > E_1$) than on the stiffer side ($E_2 < E_1$). At crack initiation, a noticeable dip in the stress intensity factor is seen suggesting a sudden release of stored energy from the initial notch. Subsequently, stress intensity factors for a growing crack increase for the case of a crack on the compliant side of sheet while a noticeable drop is seen when the crack is on the stiffer side. These can be attributed to the fact that fracture toughness of

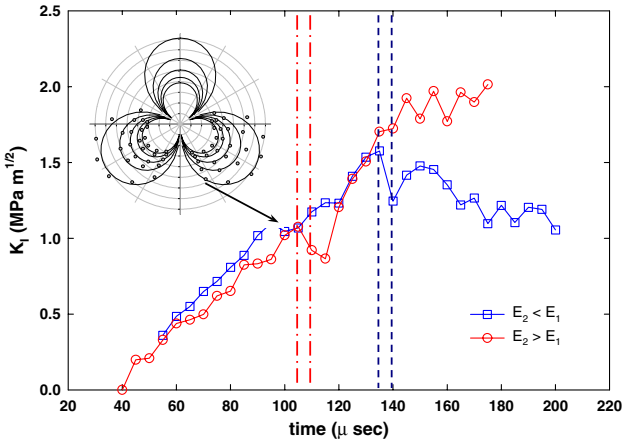

Fig. 10. Mode-I dynamic stress intensity factor histories (impact velocity = 5.8 m/s) both for crack on the compliant side ($E_2 > E_1$) and crack on the stiff side ($E_2 < E_1$). The crack initiation is indicated by the vertical bands (dash–dash: $E_2 < E_1$, dash–dot: $E_2 > E_1$). Inset shows an example of the quality of least-squares fit of the digitized data, for $E_2 > E_1$ at 100 μs.

the foam decreases as volume fraction of microballoons in the foam increases [2] as shown in Fig. 1(b).

4.2. Sandwich structures

As in the monotonically graded sheets, instantaneous crack tip positions and crack speeds were determined using the recorded images for sandwich structures with bilinearly graded as well as homogeneous core. The results are shown in Figs. 11(a) and (b). Crack initiation takes place at about 100 μs for both conventional and graded sandwich structures. As in the case of monotonically graded structure, a sharp increase in the crack speed can be noticed upon crack initiation for both the structures (see Fig. 11(b)). This is followed by an oscillatory behavior. Finally crack speed shows a decreasing trend due to impact point interaction. The crack speed characteristics are more or less similar for both sandwich constructions due to the elastic impedance equivalency between the two in the direction of crack propagation.

The stress intensity factor histories in the two cases are shown in Fig. 12. The pre-initiation data for both show monotonic increase in the stress intensity factor values up to crack initiation. Furthermore, the values for both experiments essentially overlap on each other due to the equality of average elastic impedance over the core thickness. The crack initiation occurs at approximately same value of stress intensity factor (1.5 ± 0.1 MPa $\sqrt{m}$) since the crack tip is located in a

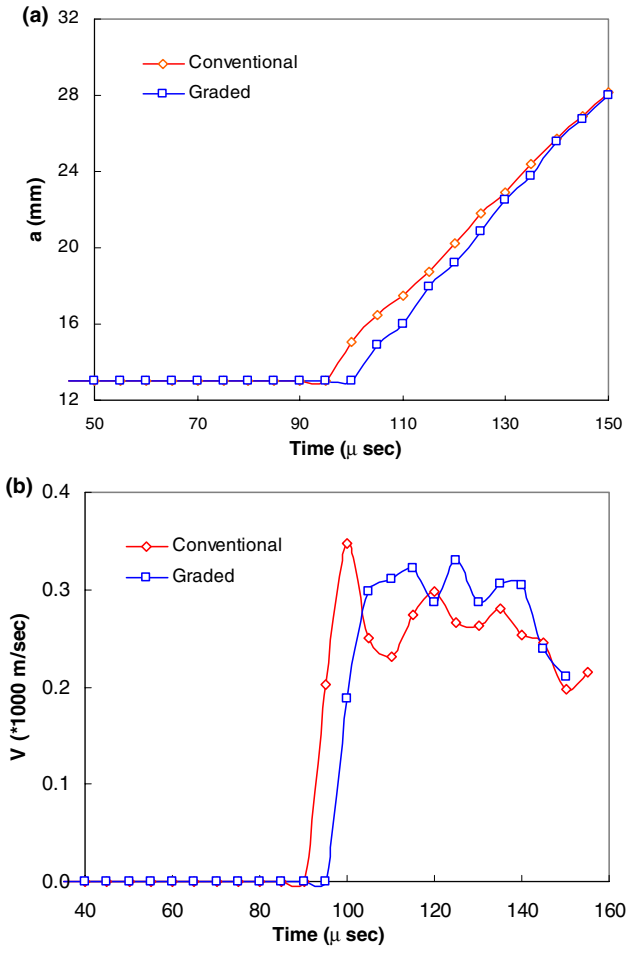

Fig. 11. Crack growth behavior in conventional and graded sandwich structures under impact loading: (a) crack growth history; (b) crack speed histories.

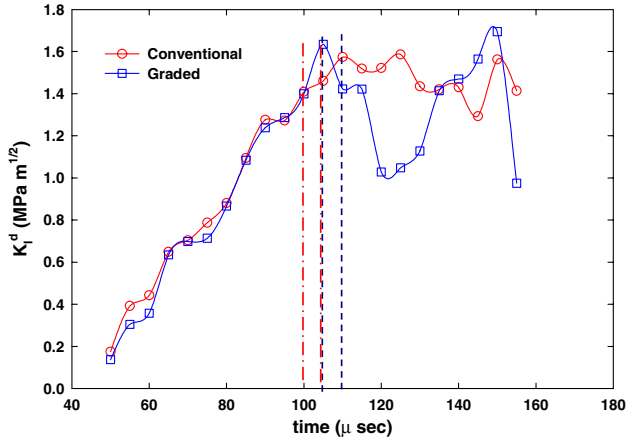

Fig. 12. Measured mode-I dynamic stress intensity factor histories for conventional and graded sandwich structures. The vertical bands (dash–dot: conventional, dash: graded) indicate crack initiation time range.

material of identical volume fraction (25%) in both cases. Following crack initiation, stress intensity factors in case of the graded core structure decrease until the

[2] Note that the values of stress intensity factors in Fig. 10 are somewhat higher than the ones in Fig. 1(b) due to higher impact velocity (5.8 m/s) and initial root radius of the notch used in optical tests.

crack tip reaches the mid-point of the core. Subsequently, an increase in stress intensity factors is evident during the window of observation. The behaviors are consistent with the post-crack initiation stress intensity factor histories of monotonically graded sheets described earlier. That is, stress intensity factors are influenced predominantly by the local volume fraction of microballoons in bilinearly graded structure. On the other hand, stress intensity factors in the conventional sandwich structure oscillate about a mean value due to a constant volume fraction of microballoons in the core. The average value, however, is approximately same as the one for the graded core. These observations are again consistent with equal average volume fraction of microballoons over the core thickness of the two architectures.

5. Finite element simulations and results: mode-I loading

5.1. Monotonically graded foam sheets

Two dimensional plane stress, elasto-dynamic finite element simulations of the experiments were undertaken. The wire mesh and the boundary conditions for the model are shown in Fig. 13. The model consisted of 8278 four noded isoparametric elements with 8463 nodes. Highly refined mesh near the crack tip also can be seen from this figure. The material property gradients were imposed on the elements using a subroutine specifically developed for the purpose. Both experimentally studied cases namely, $E_2 > E_1$ and $E_2 < E_1$, were considered. The numerical model was a free–free beam/sheet subjected to symmetric one point impact at the mid-span. In view of the symmetry of the problem only one half of the model was simulated with appropriate boundary conditions prescribed on the line of symmetry. The model was subjected to a constant velocity of 5.8 m/s according to the experimental measurements. The time integration steps were chosen such that convergence is achieved. Crack growth simulations were not considered in this work.

The stresses and displacements were extracted every 5 μs so that the results could be compared directly to the experimental counterparts. Instantaneous crack opening displacements along the crack flanks were used for extracting instantaneous mode-I stress intensity factor (K_{I}^d) values based on locally homogeneous material behavior. Using Williams' asymptotic expansion for the crack opening displacements, apparent stress intensity factors can be expressed as

$$\left[K_{\mathrm{I}}^d(t)\right]_{\mathrm{app}} \approx K_{\mathrm{I}}^d(t) + Cr, \tag{4}$$

where

$$[K_{\mathrm{I}}(t)]_{\mathrm{app}} = \sqrt{\frac{2\pi}{r}}\frac{E_0\delta_y(t)|_{\theta=\pm\pi}}{8}$$

is the apparent stress intensity factor, δ_y is the crack opening displacement, K_{I}^d is the value of mode-I crack tip stress intensity factor, E_0 is the local value of Elastic modulus at the crack tip and C is the higher order coefficient. For each time instant, values of $\widehat{K}_{\mathrm{I}}^d$ were plotted as a function of r and the extrapolated value $K_{\mathrm{I}}^d = \lim_{r\to 0}\widehat{K}_{\mathrm{I}}^d$ was evaluated as the instantaneous stress intensity factor.

It is suggested in the recent literature [27,35] that the nonsingular T-stress and hence crack tip biaxiality $\beta\left(=\frac{T\sqrt{\pi a}}{K_{\mathrm{I}}}\right)$ play an important role in the fracture

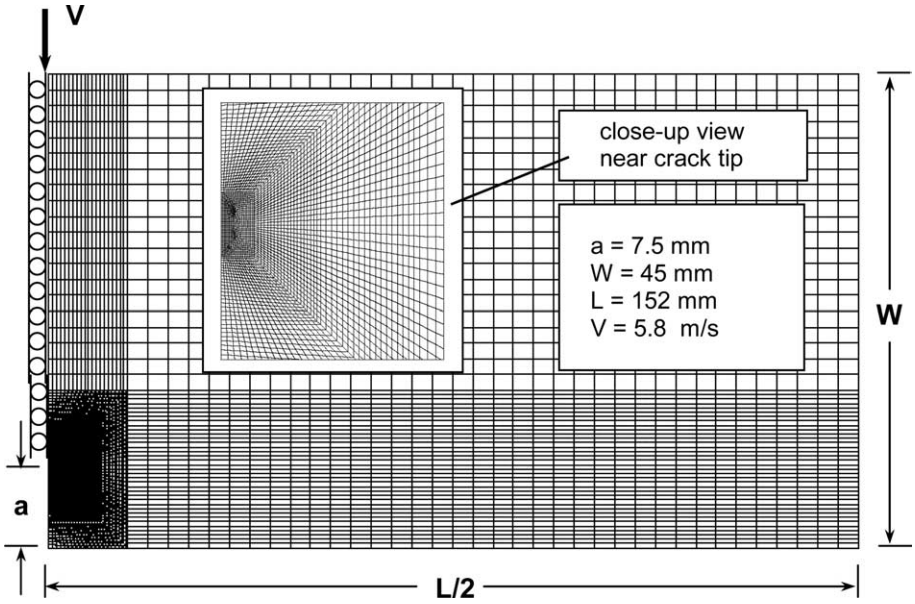

Fig. 13. Finite element mesh used for the elasto-dynamic simulation of impact failure on monotonically graded sheet.

performance of materials. In graded sheets with crack on the compliant and stiffer sides, one could potentially view the differences in failure response in terms of crack tip biaxiality. In view of simplicity of implementation, in this study T-stress calculations were made using modified stress difference method. Instantaneous normal stress difference $(\sigma_x - \sigma_y)$ ahead of the crack tip along the x-axis was used to calculate the nonsingular T-stress as

$$(\sigma_x - \sigma_y)|_{(r,\theta=0^\circ)} \approx T + Dr, \tag{5}$$

where D is a higher order coefficient. The validity of the above approaches have been demonstrated by benchmark simulations reported in [14] for K_I^d calculations and [27] for T -stress calculations.

The computed mode-I stress intensity factor and crack tip biaxiality parameter β histories are shown in Figs. 14(a) and (b). The tensile stress waves arrive at the crack tip region approximately 25 μs after impact. Subsequently, K_I^d values increase monotonically as shown in Fig. 14(a) for both the cases namely, $E_2 > E_1$ and $E_2 < E_1$. The values and the trends are similar to the ones obtained experimentally. A somewhat higher rate of increase of K_I^d initially for the crack on the compliant side of the sheet ($E_2 > E_1$) can be seen and this is similar to the observation reported in [14] for a particulate composite FGM. These differences can be potentially linked to crack tip biaxiality β. Accordingly, in Fig. 14(b) biaxiality histories are provided for completeness. The values of β are largely negative at the initial stages following impact but attain relatively stable values at later times. The values, however, are algebraically lower for the case with a crack on the compliant side of the sheet when compared to the one with a crack on the stiffer side. The higher crack tip loading rates are correlated with larger negative values of T-stress [35] and thus β.

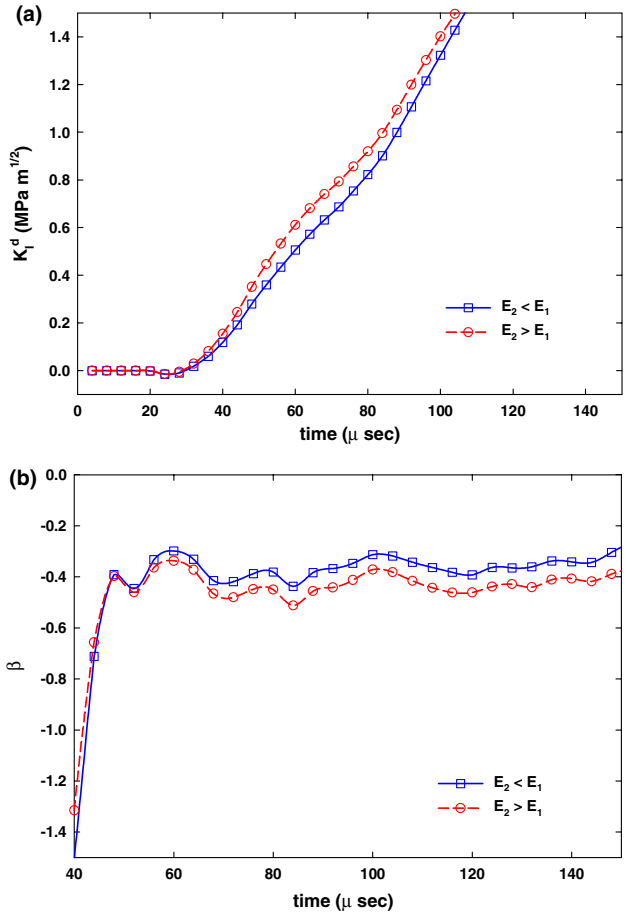

Fig. 14. (a) Mode-I dynamic stress intensity factor histories and (b) crack tip biaxiality parameter, $\beta = \frac{T\sqrt{\pi a}}{K_I}$ histories for monotonically graded sheets.

5.2. Sandwich structures

Two different plane stress, elasto-dynamic finite element models, one for a functionally graded sandwich structure and the other for a conventional sandwich structure, both equivalent in terms of average elastic impedance over the core thickness, were developed. The material properties (elastic modulus and mass density) of the former were graded with stiff layers having material properties of epoxy-rich foam (volume fraction 5%) on the outside and becoming gradually compliant towards the interior with properties in the middle that of a 45% volume fraction syntactic foam. The graded foam core was then sandwiched between two uniform epoxy layers (face-sheets thickness 3.5 mm). The imposed elastic modulus, and elastic impedance variations along the width of the model are the same ones used in the actual specimens and are shown in Fig. 4. An edge crack was introduced into each of the models as in the experiments. The crack was oriented in the direction of material property gradation and located at the mid-span of the sandwich beams. The length of the crack ($a/W = 0.31$) in each case was chosen such that the crack tip is located in a material having identical material properties in the core region. This allows a direct comparison of crack tip fracture parameters between the two models. The finite element model used for the simulation is shown in Fig. 15. The width of the graded foam core is 35 mm which is sandwiched by face sheets of 3.5 mm thick on either side. The boundary conditions for the simulations consisted of a free–free beam subjected to symmetric, constant velocity (5.8 m/s), single-point impact at the mid-span opposite to the crack tip. In view of the symmetry of the problem, again only one-half of the model was simulated for a period of ~150 μs after impact. The stresses and displacements were extracted every 5 μs for post-processing and comparison with measurements.

The K_I^d histories for both conventional and graded core sandwich structures are shown in Fig. 16. As in

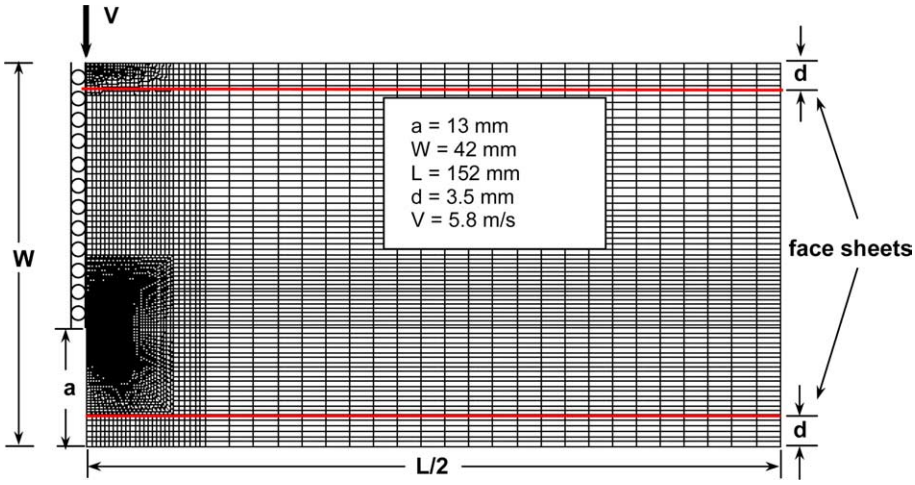

Fig. 15. Finite element model for elasto-dynamic simulation of impact damage on conventional and graded sandwich structures.

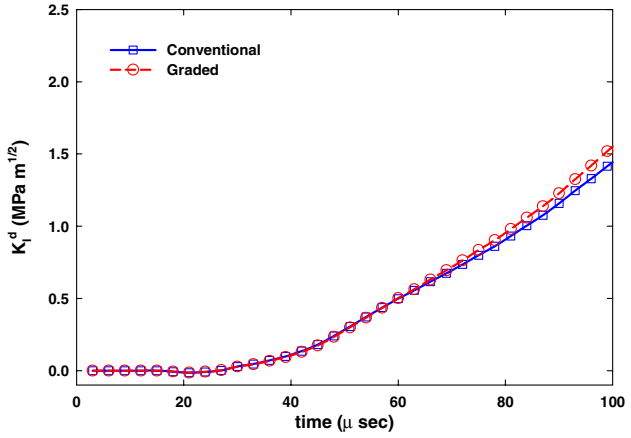

Fig. 16. Mode-I dynamic stress intensity factor histories extracted from finite element simulations for conventional and graded sandwich structures.

the monotonically graded foam case, after an initial delay in the crack tip experiencing the tensile stress waves, K_I^d values increase with time. Since the average impedance of both structures over the core depth is same, the two histories coincide with each other. This is similar to the experimental results presented in Fig. 12.

6. Face-sheet/core cracks in graded sandwich structures: mixed-mode loading

Having demonstrated the feasibility of processing and modeling sandwich structures with graded foam core, attention was next turned to investigating the benefits of functional grading on the fracture performance in the presence of face-sheet/core debonds under impact loading. Specifically, the effect of different compositional gradients in the core on crack initiation behavior of a pre-existing debond at the face-sheet/core interface experiencing a mixed-mode (mode-I and mode-II) deformations was studied. This is a more realistic configuration than the one presented in the previous sections. However, this scenario is optically challenging to address and hence undertaken only numerically using computational models previously validated by experiments. The simulated geometries were set to dimensions 152 mm × 42 mm × 8 mm, with an interface crack ($2a = 21$ mm) between the core and the face-sheet, as shown schematically in Figs. 17(a) and (b). The core width was 35 mm and the two face-sheets were 3.5 mm each. The face-sheet was again assumed to be isotropic, homogeneous and made of pure epoxy representing the stiffer layer. The core is graded from pure epoxy to 45%

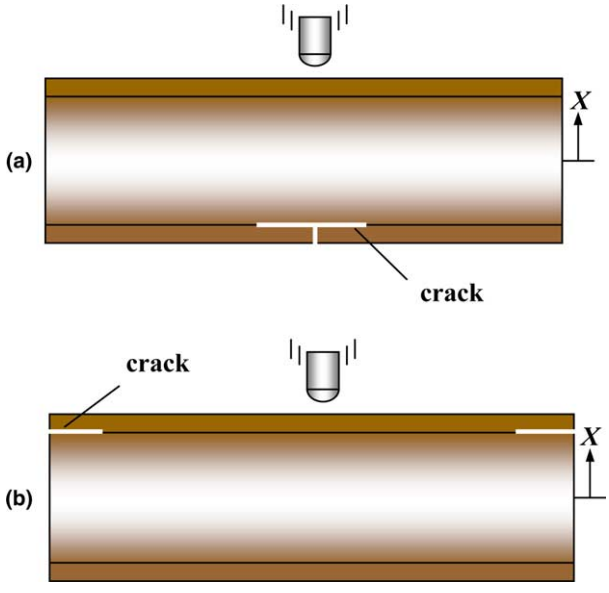

Fig. 17. Schematics of two face-sheet/core mixed-mode crack configurations in graded sandwich structure geometries used for finite element simulations: (a) centrally situated crack; (b) two edge cracks.

microballoon filled epoxy region in at the center and composition mirrored with respect to the centerline of the structure. That is, the gradient exists over the core width with location $X = 0$ (see Fig. 17) corresponding to microballoon-rich location to $X = \pm 17.5$ mm at epoxy-rich location. Accordingly, elastic modulus and mass densities were varied between 4.1 GPa and 1175 kg/m^3 ($V_f = 0$) at the face-sheet/core interface to 2.27 GPa and 648 kg/m^3 at the specimen center $X = 0$ ($V_f = 0.45$). Both these elastic properties were expressed independently using power-law descriptions:

$$E(X) = E_o + \Delta E\left(\frac{X}{W_c}\right)^n, \tag{6}$$

$$\rho(X) = \rho_o + \Delta\rho\left(\frac{X}{W_c}\right)^n, \tag{7}$$

where the subscript 'o' denotes to the material properties at the specimen center ($X = 0$), $\Delta(\cdot)$ represents the difference between the values at the center and the core–skin interface, W_c is the half-width of the core, and the exponent n provides the gradient description. The elastic modulus and mass density variations corresponding to different values of the exponent $n = 1$, 2, 4, 8, 16, and 64 are shown in Fig. 18. In this figure, $n = 1$ represents a linearly graded sandwich structure, and $n = 64$ represents the one that closely approximates a conventional sandwich structure. The average elastic impedance values $\overline{\rho C}$ for the six gradient cases of sandwich structures were calculated over the specimen height and are plotted as a function of the exponent n in Fig. 19. The average elastic impedance values over the core thickness varied between 1.65 M kg/s m^2 for the linear gradient ($n = 1$) to 1.25 M kg/s m^2 for the largest value of the exponent ($n = 64$).

The regression analysis of crack tip sliding displacements (not described here for brevity) as well as opening displacements, described earlier (Eq. (4)), was used to compute both mode-I and mode-II instantaneous

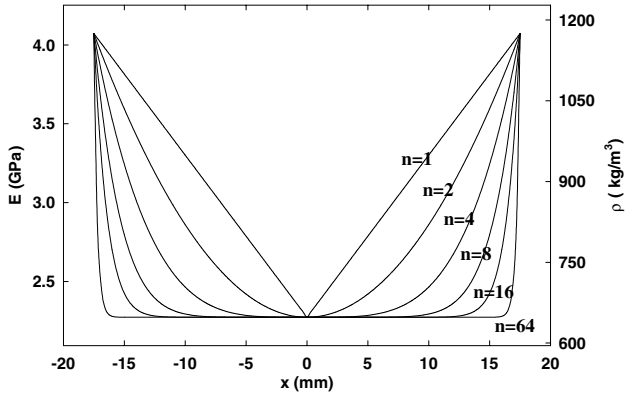

Fig. 18. Elastic modulus and density profiles used in mixed-mode finite element simulations involving face-sheet/core cracks.

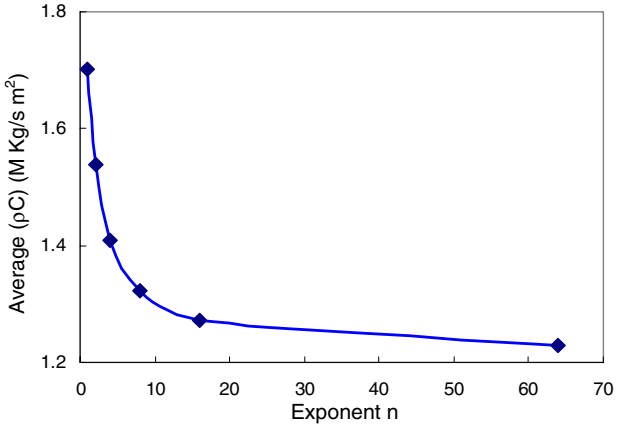

Fig. 19. Variation of average elastic impedance values for six types of sandwich structures as a function of exponent n.

stress intensity factor histories for the six different graded sandwich structures. The results are shown in Figs. 20 and 21 for the crack configurations shown in Fig. 17(a) (Case (a)) and (b) (Case (b)), respectively. The stress intensity factors are normalized using the

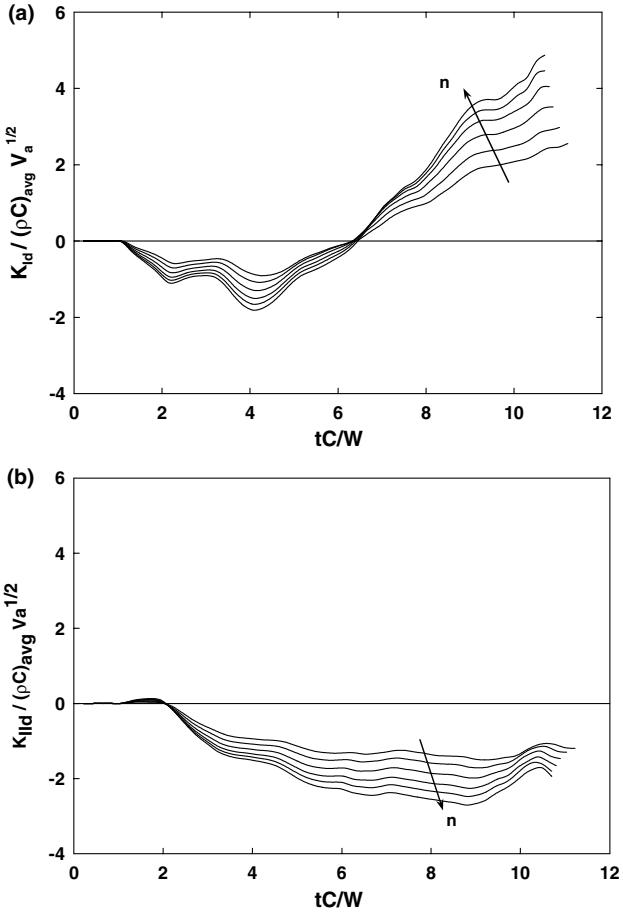

Fig. 20. Computed (FEA) dynamic stress intensity factor histories (a) mode-I and (b) mode-II, for six graded sandwich structures corresponding to Case (a) of Fig. 17.

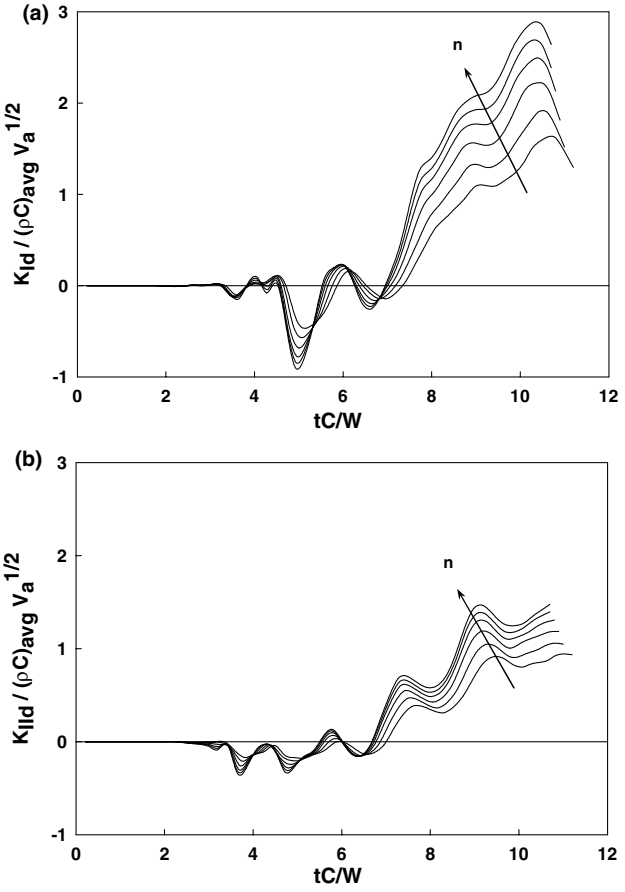

Fig. 21. Computed (FEA) dynamic stress intensity factor histories (a) mode-I and (b) mode-II, for six graded sandwich structure cases corresponding to Case (b) of Fig. 17.

average impedance $\overline{C\rho}$, the impact velocity V, and the square root of the crack length a. Similarly the time is normalized using average dilatational wave speed of the graded sandwich structures and the specimen height: $T = t\bar{C}_l/W$, where $\bar{C}_l$ is the average longitudinal wave speed.

Case (a) Significant values of stress intensity factors are observed beyond $T \sim 1$ for all six different gradations of core properties, after the reflected tensile stress waves reach the crack tip, and are followed by monotonic increase in stress intensification. The mode-I stress intensity factors are initially negative up to $T \sim 6.5$ suggesting tendency for the crack tip to close during this time period. Beyond that, the values become positive and there is a monotonic increase in the mode-I stress intensity factor at different rates, the lowest for linearly graded core ($n = 1$) and highest for the one closest to the homogeneous core ($n = 64$). The mode-II stress intensity factors on the other hand are negative throughout the observation window and continuously increase in magnitude up to approximately $T \sim 9$ after which a drop in the values is evident. Again, the magnitude of mode-II stress intensity factors are consistently higher for $n = 64$, the one closest to the conventional core sandwich structure when compared bilinearly graded core ($n = 1$). Thus, one can deduce that for a given value of critical energy release rate or effective stress intensity factor, crack initiation would occur more readily in the conventionally graded architecture compared to the bilinearly graded one. Other gradations described by different values of n are bounded by these two cases.

Case (b) In Figs. 21(a) and (b), crack tip stress intensity factors are discernible after nondimensional time $T \sim 3$. Both mode-I and -II stress intensity factors are oscillatory up to $T \sim 7$ during which time the crack tip is experiencing relatively small values of K_I and K_{II} compared to the ones at later times. Further, both stress intensity factors are consistently negative suggesting crack tip sliding accompanied by closure during this period. Beyond this oscillatory time period, both K_I and K_{II} values monotonically increase and K_I is positive suggesting crack opening. The rate of increase of stress intensity factors vary from being lowest for the graded core with exponent $n = 1$ and highest when $n = 64$. This suggests that a bilinearly graded core reduces stress intensification near the crack tip compared to the homogeneous core with all other variations bounded between these two situations. It can also be noticed that the magnitude of stress intensity factors during the time period is relatively small compared to the ones in Case (a) (Fig. 20). Additionally, K_{II} in this case are positive unlike Case (a).

7. Discussion

The experimental results from monotonically graded foam specimens with crack along the compositional gradient (mode-I) suggest that crack initiates earlier and propagates at a higher average velocity when the crack is situated on the compliant side of the sample ($E_2 > E_1$) when compared to the one with a crack on the stiffer side ($E_2 < E_1$). The stress intensity factors for growing cracks increase in the former case while a decreasing trend is seen in the latter since fracture toughness of the foam decreases with increasing volume fraction of microballoons. This behavior is consistent with previous investigations where in solid glass filled epoxy composites [14,15] were used. The finite element simulations show a higher rate of crack tip loading when the crack is located on the compliant side. The differences between the two crack configurations are linked to the differences in crack tip constraints through finite element analysis.

In case of homogeneous and bilinearly graded foam core sandwich structures of equivalent elastic impedance and with cracks along to the gradient (mode-I), the crack initiation time and crack growth behaviors are essentially same. Further, the pre- and post-crack initiation stress intensity factor histories are also well

matched in an average sense although stress intensity factor history in the graded core is relatively more oscillatory as one could expect. Thus it can be argued that pertaining to mode-I fracture, the beneficial aspects of conventional sandwich structures can be fully preserved in the graded architecture. At the same time, interfacial separation between the face-sheet and the core, in a graded core sandwich can be suppressed. Beyond these, no other fracture related benefits are evident.

The beneficial effects of compositional grading of the core of sandwich structures are evident more prominently in the analyses of cracks normal to the compositional gradient (mixed-mode crack) and located at the face-sheet/core interface. Plane elasto-dynamic numerical simulations corresponding to two interfacial crack configurations show consistent reduction in stress intensity factors when the core is graded compared to conventional homogeneous core counterpart under stress wave loading. Based on the magnitude of normalized stress intensity factors, the configuration with a centrally located split-crack (Case (a)) at the lower interface is relatively undesirable of the two configurations modeled. The mode-II stress intensity factor in this case is negative throughout the window of observation while its mode-I counterpart turns positive at later times. Thus, if the crack initiation were to occur at later times, the crack would tend to grow into the core material. The other configuration (Case (b)) also shows the same tendency at later time as both mode-I and -II components are positive. It may be worth noting that, since mode-I stress intensity factors are initially negative, one could conjecture that if the face-sheet/core cracks were to initiate at earlier times, it would likely be as shear cracks as evident in the work reported in [6].

8. Conclusions

Feasibility of using functionally graded foam as core material in sandwich construction for impact loading conditions is demonstrated using model sandwich structures comprising of graded core with a bilinear volume fraction variation. For comparative purposes, a conventional sandwich with a homogeneous core is also developed. The two models are intentionally made dynamically equivalent by equalizing average elastic impedance over the height of the core in both designs. The results are supplemented by crack initiation and growth behavior studies in monotonically graded sheets for understanding crack growth pattern in the graded core of the sandwich structure. The real-time optical measurements show that:

- In case of monotonically graded foams, mode-I stress intensity factors increase when the crack grows from the compliant side to the stiffer while the opposite occurs when the growth is from the stiffer side to the compliant. This is mainly attributed to reduction in fracture toughness with increasing microballoon volume fraction in the foam and the differences in the crack tip constraint.
- The crack growth in the bilinearly graded core with a crack along the gradient direction shows decreasing mode-I stress intensity factors until the crack reaches the mid-point of the core. Subsequently, an increasing trend is seen as the crack grows into stiffer material. The sandwich structure with a homogeneous core of equivalent elastic impedance shows that crack growth in the core occurs at approximately constant stress intensity factor, unlike in the graded counterpart.
- Pre-initiation mode-I stress intensity factor histories for both graded and homogeneous core sandwiches show nearly similar fracture response. However, delamination at face-sheet/foam core interface is observed only in conventional sandwich structure. Thus, functional grading seems to preserve the benefits of conventional core foams while suppressing face-sheet/core delamination during impact loading.

Finite element models have successfully captured the experimental responses up to crack initiation. Using these models, role of different elastic impedance gradients in the core material for two cracked sandwich structural geometries with mixed-mode, face-sheet/core cracks are examined. Computations suggest enhanced fracture performance of graded sandwich structures when compared to a conventional counterpart under stress-wave loading conditions. The elastic impedance gradients, characterized by the power-law exponent, indicate that the crack tip loading rates as well as mixed-mode crack tip stress intensity factors are both consistently lower for lower exponent values ($n \geqslant 1$).

Acknowledgement

Authors would like to thank US Army Research Office for supporting the research through grant # DAAD 19-01-1-0414 (Dr. Bruce LaMattina, Program Director).

References

[1] Zenkert D. Handbook of sandwich construction. West Midlands: Cradley Heath; 1997.
[2] Nemes JA, Simmonds KE. Low-velocity impact response of FOAM-core sandwich composite. J Comp Mater 1992;26(4):500–19.
[3] Kosza P, Sayir MB. Failure parameters in the core of sandwich structures under impact loading. Int J Impact Eng 1994;15(4):501–17.
[4] Wu CL, Sun CT. Low velocity impact damage in composite sandwich beams. Comp Struct 1996;34(1):21–7.

[5] Shipsha A, Hallstrom S, Zenkert D. Failure mechanisms and modeling of impact damage in sandwich beams – a 2D approach: Part I – Experimental investigation. J Sandwich Struct Mater 2003;5(1):7–31.
[6] Xu LR, Rosakis AJ. Impact failure characteristics in sandwich structures Part I: Basic failure mode selection. Int J Solids Struct 2002;39(16):4215–35.
[7] Bishop A, Navaratnam M, Rawlings RD, McShane HB. Functionally gradient material produced by a power metallurgical process. J Mater Sci Lett 1993;12:1516–8.
[8] Koizumi, Niino M. Overview of FGM research in Japan. MRS Bull 1995;20:19–21.
[9] Butcher RJ, Rousseau C-E, Tippur HV. A Functionally graded particulate composite: Preparation, measurements and failure analysis. Acta Mater 1998;47(1):259–68.
[10] Parameswaran V, Shukla A. Processing and characterization of a model functionally gradient material. J Mater Sci 2000:21–9.
[11] Venkataraman S, Sankar BV. Elasticity solution for stresses in a sandwich beam with functionally graded core. AIAA J 2003;41(12):2501–5.
[12] Nakamura T, Wang ZQ. Simulations of crack propagation in graded materials. Mech Mater 2004;36:601–22.
[13] Marur PR, Tippur HV. Dynamic response of bimaterial and graded interface cracks under impact loading. Int J Fract 2000;103:95–109.
[14] Rousseau C-E, Tippur HV. Dynamic fracture of compositionally graded materials with cracks along the elastic gradient experiments and analysis. Mech Mater 2001;33:403–21.
[15] Rousseau C-E, Tippur HV. Influence of variations on crack initiation in functionally graded glass-filled epoxy. Eng Fract Mech 2002;69:1679–93.
[16] Parameswaran V, Shukla A. Dynamic fracture of a functionally gradient material having discrete property variation. J Mater Sci 1998;33:3303–11.
[17] Malloy RA, Hudson JA. In: Lee SM, editor. International encyclopedia of composites. VCH Publications; 1990.
[18] Shutov FA. Syntactic polymer foams. In: Klempner D, Frisch KC, editors. Handbook of polymeric foams and foam technology. New York: Hanser Publishers; 1991.
[19] Gupta N, Kishore, Woldensenbet E, Sankaran S. Studies on compressive failure features in syntactic foam material. J Mater Sci 2001;36:4485–91.
[20] Gibson L, Ashby MF. Cellular solids: Structures and properties. Cambridge University Press; 1997.
[21] Vural M, Ravichandran G. Microstructural aspects and modeling of failure in naturally occurring porous composites. Mech Mater 2003;35:523–36.
[22] El-Hadek M, Tippur HV. Measurement and modeling of mechanical properties of microballoon dispersed epoxy and urethane: implications for studying porosity. J Mater Sci 2002;37(8):1649–60.
[23] Ishai O, Hiel C. Damage tolerance of a composite sandwiches with interleaved foam core. J Comp Technol Res 1992;14(3):155–68.
[24] Hiel C, Dittman D, Ishai O. Composite sandwich construction with syntactic foam core: a practical assessment of post-impact damage and residual strength. Composites 1993;24(5):447–9.
[25] Scarponi C, Briotti G, Barboni R, Marcone A, Iannone M. Impact testing on composites laminates and sandwich panels. J Comp Mater 1996;30(17):1873–911.
[26] Dally JW, Sanford RJ. Strain-gage methods for measuring the opening-mode stress intensity factor, K_I. Exp Mech 1987;49:381–8.
[27] Maleski MJ, Kirugulige MS, Tippur HV. A method for measuring mode-I crack tip constraint under static and impact loading conditions. Exp Mech 2004;44(5):522–32.
[28] Bao G, Cai H. Delamination cracking in functionally graded coating/metal substrate systems. Acta Mater Mater 1997;45(3):1055–66.
[29] Lee Y, Erdogan F. Residual thermal-stresses in FGM and laminated thermal barrier coatings. Int J Fract 1994;69(2):145–65.
[30] Gu P, Asaro R. Cracks on functionally graded materials. Int J Solids Struct 1997;34(1):1–17.
[31] Marur P, Tippur HV. Numerical analysis of crack-tip fields in functionally graded materials with a crack normal to the elastic gradient. Int J Solids Struct 2000;37:5353–70.
[32] Meyers MA. Dynamic Behavior of Materials. John Wiley; 1994.
[33] Tippur HV, Krishnaswamy S, Rosakis AJ. A coherent gradient sensor for crack tip measurements: analysis and experimental results. Int J Fract 1991;48:193–204.
[34] Parameswaran V, Shukla A. Crack-tip fields for dynamic fracture in functionally gradient materials. Mech Mater 1999;31:579–96.
[35] Jayadevan K, Narasimhan R, Ramamurthy T, Dattaguru B. A numerical study in dynamically loaded fracture specimens. Int J Solids Struct 2001;38:4987–5005.